

# Dynamic pH mapping in microfluidic devices by integrating adaptive coatings based on polyaniline with colorimetric imaging techniques†

Larisa Florea, Cormac Fay, Emer Lahiff, Thomas Phelan, Noel E. O'Connor, Brian Corcoran, Dermot Diamond and Fernando Benito-Lopez\*

5 Received (in XXX, XXX) Xth XXXXXXXXXX 20XX, Accepted Xth XXXXXXXXXX 20XX

DOI: 10.1039/b000000x

In this paper we present a microfluidic device that has integrated pH optical sensing capabilities based on polyaniline. The optical properties of polyaniline coatings change in response to the pH of the solution that is flushed inside the microchannel offering the possibility of monitoring pH in continuous flow over a  
10 wide pH range throughout the entire channel length. This work also features an innovative detection system for spatial localisation of chemical pH gradients along microfluidic channels through the use of a low cost optical device. Specifically, the use of a microfluidic channel coated with polyaniline is shown to respond colorimetrically to pH and that effect is detected by the detection system, even when pH gradients are induced within the channel. This study explores the capability of detecting this gradient by  
15 means of imaging techniques and the mapping of the camera's response to its corresponding pH after a successful calibration process. The provision of an inherently responsive channel means that changes in the pH of a sample moving through the system can be detected dynamically using digital imaging along the entire channel length in real time, without the need to add reagents to the sample. This approach is generic and can be applied to other chemically responsive coatings immobilised on microchannels.

## 20 Introduction

Conventional glass-type electrodes have been widely used for pH measures for many years in both industry and academic areas. However, in terms of specific applications (*e.g.* in vivo, food industry, or for clinical applications), they possess several  
25 disadvantages due to their size constraints, rigidity, and the inflexibility of the glass electrode. In recent years, a wide number of pH sensors have been developed to overcome these limitations, including ion sensitive field-effect transistor (iSFET) pH sensors<sup>1-4</sup>, optical pH sensors based on pH responsive dyes<sup>5-8</sup>, hydrogel  
30 film pH sensors<sup>9, 10</sup>, and solid-state metal oxides pH sensors<sup>11-13</sup>. In particular, optical pH sensors present several advantages over the traditional pH electrodes as such their low costs, immunity from electromagnetic field, absence of electric contacts, possibility of reference electrode removal and a high degree of  
35 miniaturisation<sup>14</sup>. Optical fiber-based pH sensors have been particularly popular, as the fibre allows the optical signal to be transported over long distances, which can facilitate applications in remote sensing<sup>15</sup>.

Usually, these optical pH sensors (or optrodes) employ a dye  
40 or an indicator that requires immobilisation onto a solid support material. There are several critical issues related to this approach: firstly, the dye should retain its optical properties after the immobilisation process<sup>16</sup> and secondly, it should not leach into the solution<sup>17</sup>. A third issue of practical importance is their  
45 inherently narrow dynamic response range which is usually around 3-4 pH-units centred on the dye's pKa<sup>18</sup>.

Therefore, the further improvement of such sensors focuses on the search for new materials that can overcome these issues. An alternative approach is to use the inherent optical response of  
50 certain polymers like the conducting polymer polyaniline (PAni)

rather than a conventional pH-sensitive dye. PAni displays striking changes in the visible/NIR spectrum upon proton-mediated doping-dedoping of the polymer backbone, thus offering the possibility of developing optical sensors with  
55 extended pH ranges. The polymer itself, therefore, acts as both the matrix support and the indicator dye. In this way, leaching is prevented, thereby enhancing the long-term stability and reproducibility.

PAni is an excellent candidate for the fabrication of optical  
60 sensors in the visible-near IR detection since it is an intrinsically pH-sensitive polymer with good environmental stability<sup>19, 20</sup>. Furthermore, by focusing on PAni nanofibres we can dramatically increase the surface area of the material<sup>21</sup>, which in turn can manifest in improved response times and sensitivity.

A relatively new and promising approach to produce sensors of this kind involves optofluidics wherein optical and fluidic functionalities are integrated at the micro- and nano-scale to leverage their combined advantages by functionalising the inner walls of a microchannel with a responsive material<sup>22, 23</sup>. For  
70 example, functionalisation with antibodies for flow-through cell separation have been reported<sup>24</sup>, as have fluorescent dyes for optical sensing of acidity<sup>25</sup> and monolayers that exhibit metal ion sensing properties<sup>26, 27</sup>.

Nowadays, a wide variety of detectors can be employed to  
75 transduce the colorimetric analytical signal, such as light dependent resistors<sup>28, 29</sup>, photodiodes<sup>30-32</sup>, phototransistors<sup>33-35</sup> and even reverse-biased LEDs<sup>36-38</sup>. More specific to this study is the use of digital imaging cameras for the detection of colorimetric reactions. Up to now, almost all of the studies carried out have  
80 been based on the RGB colour model, probably because this is readily accessible via a number of popular image processing

packages<sup>39-43</sup>. The major challenge with this approach is that the RGB colour space is inherently sensitive to changes in ambient lighting, and measurements therefore have to be made under strictly controlled light conditions. Recently, studies such as those by Fay *et al.*<sup>44</sup> (qualitatively) and Cantrell *et al.*<sup>45</sup> (quantitatively) explored the use of a different colour model (HSV) for colorimetric chemical analysis which has shown to be more tolerant of ambient light variations<sup>46</sup>.

Based on this concept, we present an innovative, robust, simple and fast method to measure pH simultaneously at all locations across an entire microfluidic system using polyaniline nanofibres modified microchannel coupled with HSV-based digital image color analysis.

## Experimental

### Microfluidic device fabrication

The fabrication of the master mold was carried out using a laser ablation system-excimer/CO<sub>2</sub> laser (Optec Laser Micromachining Systems, Belgium) by cutting the microfluidic structures in a 50 μm double-sided pressure sensitive adhesive film, PSA, (AR8890, Adhesives Research, Ireland) and pasting one of the PSA sides to a petri dish<sup>47</sup>.

For PDMS casting, the precursor was prepared by mixing PDMS elastomer with the curing agent from Sylgard 184 kit at a weight ratio of 10:1, poured onto a master mould, and cured in an oven at 80 °C for 2 h. Following curing, the PDMS layer is peeled from the master. The inlets and outlets (800 μm in diameter) were made using a manual puncher (Technical Innovations, Inc., Brazoria, TX). The PDMS replica (~ 1 mm height) was thoroughly washed with isopropanol and exposed to oxygen plasma to seal the chip to a clean glass slide (35 mm x 64 mm, Agar Scientific Limited, England) or another flat PDMS layer (~ 2 mm height). Silicon tubes were employed to further connect the main inlets with a syringe pump (PHD 2000 Syringe, Harvard Apparatus) for sample delivery and washing.

### Microfluidic device functionalisation

The functionalisation of the inner walls of the microfluidic channel with PANi nanofibres was achieved using the procedure described in Figure 1. The detailed microchannel functionalisation process and the corresponding characterisation of the coating are listed in the ESI†. Briefly, immediately after exposure of the PDMS chips to oxygen plasma for 60 s (Harrick Plasma) and sealing to the glass slide/PDMS layer, the activated channels (1000 × 100 μm) were flushed with a 20% wt solution of *N*-[3-(trimethoxysilyl) propyl]aniline in ethanol for 60 min at a flow rate of 0.5 μL min<sup>-1</sup>. Using this technique, a monolayer of silane-bearing aniline was formed on the substrate via molecular self-assembly. Chemical deposition of the PANi on the modified microchannel walls was performed by filling the microchannel with freshly prepared 1 M HCl solution containing the oxidant (ammonium peroxydisulfate) and aniline in a molar ratio of 0.25:1. This molar ratio was chosen as it has been previously shown that polymerisation of aniline in these experimental conditions produces nanofibres<sup>48</sup>. The pendant aniline on the surface served as the initiation site for polymerisation and was also used to covalently anchor the PANi chain on the substrate<sup>49</sup>.

The polymerisation time was fixed to 20 h. After polymerisation, the channels were washed extensively with water to remove any unattached polyaniline nanofibres. The resulting films had good adhesion due to the chemical bonding between the substrate and polymer film. Homogeneous PANi coatings were obtained, covalently attached to the internal walls of microchannels made of PDMS/PDMS or PDMS/glass, see Figure 2.

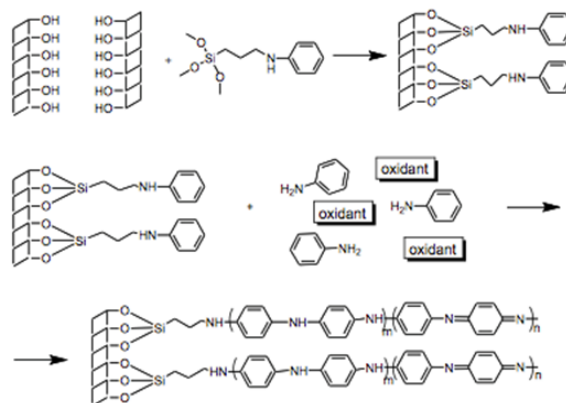


**Figure 1.** Chemical functionalisation of microchannel surface with polyaniline chains.

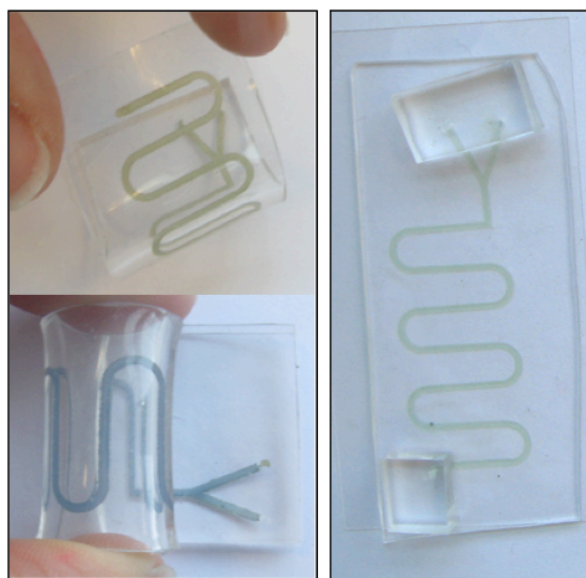


**Figure 2.** Pictures of polyaniline functionalised PDMS/PDMS (left), acidic on the top and basic on the bottom, and glass/PDMS (right) microfluidic devices. The picture on the right shows the PDMS extensions that were attached to the PDMS layer by oxygen plasma. These extensions were configured to secure the connections between the silicon tubes and the inlets of the microchannel and to facilitate sample delivery.

### Measurement of absorbance spectra of PANi coatings

Changes in the absorbance spectra of the PANi coatings as different pH solutions flushed inside the microchannel were recorded using two fiber-optic light guides connected to a Miniature Fiber Optic Spectrometer (USB4000 - Ocean Optics)

and aligned using an in-house made holder. The in-house-designed holder was fabricated using a 3D printer (Dimension SST 768) in black acrylonitrile butadiene styrene co-polymer (ABS) plastic in order to minimise interferences from ambient light. The two parts of the holder (2 identical parts, one to be placed on top of the microfluidic chip, the other underneath) were designed using ProEngineer CAD/CAM software package and fixed together with screws ensuring precise alignment between the two fiber-optics (ESI – Fig. S1).

The Absorbance spectra recorded with Miniature Fiber Optic Spectrometer (USB4000). For clarity, all absorbance spectra recorded were smoothed using Origin software using Savitzky-Golay algorithm.

### Digital image capture

After the fabrication of the flow channels and subsequent analysis using reference instrumentation (spectrophotometer) the channels were then subjected to analysis via digital imaging techniques. The channel was placed within the field of view of a standard colour camera (Panasonic DMC-FZ38) along with a white background for subsequent image processing. An XRite professional colour reference chart was also placed within the camera's field of view (see ESI† - Figure S2) as this experiment was performed under variable ambient lighting conditions.

Solutions of known pH produced by mixing appropriate amounts of hydrochloric acid or sodium hydroxide (pH 2 to 12) were then flushed through the microchannel at a flow rate of 50  $\mu\text{L min}^{-1}$ . At each pH unit step, an image was captured using the colour camera. This process was repeated and multiple images gathered at each unit step to investigate reproducibility.

An additional set of images were similarly captured, in which the flow channel was first filled with a solution of pH 3 and then a droplet of pH 6.5 aqueous solution placed at the opposite inlet where it was encouraged along the microchannel via an applied negative pressure using a microsyringe. This generated a pH gradient inside the microchannel along the channel's length. Therefore, the channel showed two extreme colours at either end coupled with a colour gradient connecting them. The ability to detect this pH gradient point through image processing and analysis was then investigated.

### Image processing

A number of image processing steps were employed in order to analyse the overall channel pH for the calibration procedure, and subsequently additional steps were undertaken to detect the pH gradient along the channel. After capturing an image (see ESI† - Figure S2a) a segmentation process identified regions of interest from background areas (see ESI† - Figure S2b). The regions were identified based on their spatial coordinates and were matched between progressive calibration images on this basis. The average Hue component of each region was taken to represent the colour of the channel and reference patches, which were then used for normalisation, and later to generate a calibration plot. Following this, a similar approach was employed to analyse the pH gradient along the channel in which the pH analysis was localised at every point along the channel. A more detailed account of these

processing steps can be found within the accompanying supporting information.

## Results and discussion

### Characterisation of the PANi coatings

The PANi coatings were characterised by Raman spectroscopy as it permits in situ analysis<sup>50</sup> of PANi coating inside the microchannel (see ESI† - Figure S4). Raman spectroscopy showed that PANi is obtained in its half-oxidised emeraldine state<sup>51</sup>. In addition, Raman spectroscopy was also employed to study the changes in the bonding structure of the coatings upon doping-dedoping, as very distinct signature bands appear for the quinoid and benzenoid rings, respectively<sup>52, 53</sup>. When a solution of pH 2 is passed through the microchannel, PANi presents the typical bands for the emeraldine salt (ES). When a solution of pH 12 is flushed through the microchannel, the ES bands decrease and the specific quinoid ring bands appear in the spectra, reflecting the dedoped state – emeraldine base (EB).

Scanning electron microscope (SEM) images showed that using the polymerisation technique described in the experimental section, PANi nanofibres were obtained, covalently attached to the inner walls of the microchannels, (Figure 3). The immediate advantages of having nanofibres (*versus* bulk PANi) are the high surface area that is exposed to the target molecules and the very short diffusional path lengths<sup>54</sup> which produces enhanced sensitivity coupled with fast response times<sup>21,55, 56</sup>.

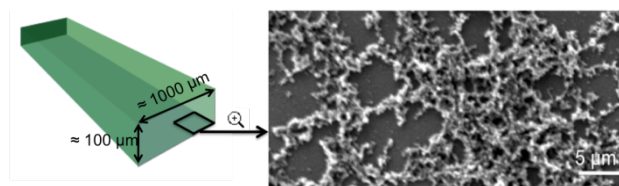


**Figure 3** Representation of the polyaniline functionalised microchannel (left). SEM image of the polyaniline functionalised glass bottom layer showing a homogeneously covered surface with polyaniline nanofibres (right).

### pH measurements

Polyaniline's sensitivity towards pH has been extensively used in recent years for the development of pH sensors due to its intrinsic doping-dedoping pH response<sup>57, 58</sup>. However, to the best of our knowledge this is the first example of the use of polyaniline nanofibres as a pH optical sensor in a microfluidic device, wherein the whole inner wall of the microchannel acts as a sensor enabling the pH to be measured simultaneously at all points within the channel.

The reversible protonation/deprotonation reaction of PANi is of particular interest during the development of the pH sensor. The process occurs on the imine nitrogen atoms as shown in ESI† - Figure S5. The transformation of Emeraldine Salt (ES) to Emeraldine Base (EB) by deprotonation is accompanied by significant changes in colour. This phenomenon is observed in the case of the PANi coatings when colourless solutions of at varying pH are passed through the microchannel, showing the ability of the covalently bonded PANi nanofibres to rapidly respond to changes in their environment (see ESI† - Figure S5).

The changes in the absorbance spectra of the PANi coatings in response to different pH solutions flushed inside the microchannel were recorded using two fiber-optic light guides connected to a Miniature Fiber Optic Spectrometer and aligned using an in-house made cell.

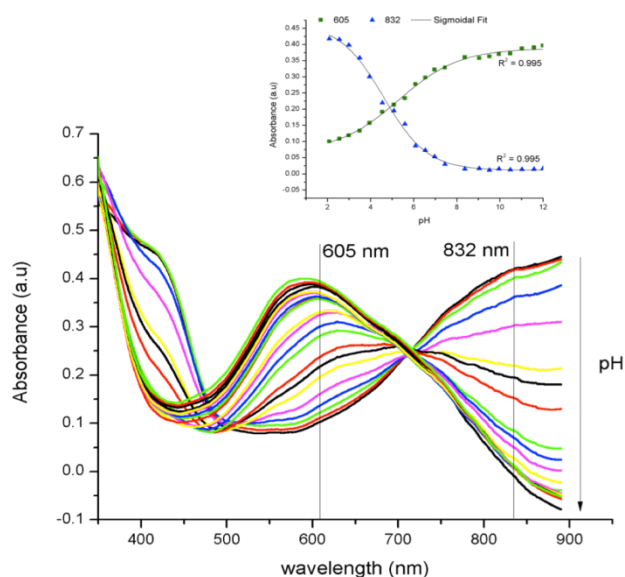


**Figure 4.** Absorbance spectra of the polyaniline coatings in the channel when solutions at different pH are passed through (pH 2-12). Inset - Graph of the absorbance change of polyaniline coatings vs. pH at 605 nm and 832 nm.

The UV-VIS absorption spectra of PANi films were measured for each pH solution passed through the channel at a flow rate of 50  $\mu\text{L min}^{-1}$ , see Figure 4. It is important to note that the absorbance spectrum changes very rapidly after the solution reaches the detection area (approx. 2 s), thereby ensuring a very fast response of the device (see ESI† - videos 1 and 2). Moreover, the signal remains stable during the timescale of the experiment, which was set to 5 minutes. The measurements were done in triplicates with a standard deviation of the absorbance value over the calibration range of 0.001.

As depicted in Figure 4 the spectrum of the PANi coatings is highly pH dependent and changes in colour from the green (ES) to blue (EB). Increasing the pH from 2 to 12 leads to a shift in the absorption  $\lambda_{\text{max}}$  of PANi in the visible region from 420 nm (at pH 2) to 605 nm (at pH 12). This shift is due to doping-dedoping of PANi coatings and can be explained by the different degree of protonation of the imine nitrogen atoms in the polymer chain<sup>59</sup>. More specifically, in a low pH environment, PANi exhibits strong absorbances at approximately 420 nm and 830 nm assigned to polaron and bipolaron transitions. Upon dedoping these transitions disappear and a new absorbance band appears at approximately 600 nm. This new band is ascribed to the exciton formation in the quinonoid rings<sup>60</sup> and it is responsible for the blue colour of the PANi coatings. The pH dependence of the absorptions at 605 nm and 832 nm were plotted in Figure 4 - Inset. The characteristic PANi sigmoid shape curve ( $R^2 = 0.996$ ) was obtained for the absorbance change versus pH, similar to the previous reported results in the case of PANi<sup>19, 51</sup>. The curve is broad, ensuring that the pH dependence of the PANi occurs over a wide range of pH. Therefore, this type of coating can be used for

pH sensing across a reasonably broad range, constituting an important advantage over common pH indicator dyes. Since PANi does not fit the expected response curve for an indicator, because of its broad range, the Henderson-Hasselbach equation cannot be applied<sup>7</sup>. In the literature, there have been attempts to introduce an adjusted exponent to fit PANi doping- dedoping behaviour using Henderson-Hasselbach equation, although these attempts were proven to be unsuccessful<sup>58</sup>. Therefore, only an apparent  $pK_a$  value can be used to describe the sensor response. As depicted from Figure 4 - Inset, the apparent  $pK_a$  value of PANi coatings is approximately 5, representing the pH value where the two sigmoids intersect (concentration of ES is approximately equal with the concentration of EB). Most probably this value represents a distribution of  $pK_a$ 's of PANi units with differing chain length and local environments<sup>57</sup>. Nevertheless, since important changes in  $\lambda_{\text{max}}$  and absorbance were observed in the pH range from 2 to 8, it should be possible to use these PANi coated microchannels for monitoring the pH of, for instance, physiological fluids (gastric juice, saliva, blood) which are important applications for microfluidics at this time.

### pH determination via colorimetric imaging analysis

It has been shown that the channels respond accurately to changes in pH when analysed using a spectrophotometer. However, this work also explored the possibility of performing colorimetric analysis without the need for specialised instrumentation *i.e.* through the use of a standard digital colour camera. This has the potential to extend the applicability of the sensor, for instance, to point of care microfluidic devices and to low cost diagnostics for the developing world using mobile phones with integrated digital cameras to capture analytical information<sup>61</sup>. The steps taken to extract colorimetric information from the captured images are outlined in detail in the ESI†.

Processing of the images began with the application of a white balance algorithm. This was possible as the image setting/scene was relatively similar in each case, and included a white region specifically for this purpose. As this study took place in an ambient lighting environment, normalisation of the images in this way was necessary to compensate for shifts in ambient light intensity. For further robustness, the Hue value representing the colour of the channel underwent a colour normalisation process using two of the array of invariant reference patches (*i.e.* the purple and yellow patches as presented in Figure S2). Next, the average and standard deviation of the channel's normalised Hue value across each of the captured images at corresponding pH unit steps were calculated ( $\text{RSD} \leq 2.06\%$ ). Following this, a calibration plot of the camera's response to different pH solutions was achieved and a sigmoidal model was applied to the data points, see ESI† - Figure S6. It can be seen from the figure that an excellent fit was achieved ( $R^2 = 0.998$ ,  $n = 18$ ) and subsequently, the resulting mathematical model was used to map the camera response to pH concentration values for gradient analysis.

While spectrophotometer and the camera generate the pH estimations on the basis of 'colour' measurements, the way in which this is achieved is different for both devices. The spectrophotometer can generate a calibration plot at any effective wavelength (*i.e.* regions of the absorbance spectrum of the dye that change with pH) within its measurement range. For this

study, the most dominant peak changes were selected; 605 nm and 832 nm, see Figure 4. In contrast, the camera measures colour across the entire available spectrum, and wavelength specific measurements are not possible except through the rather crude RGB division of the spectrum into three 'Red', Green' and 'Blue' (RGB) channels. When conversion into the HSV colour space is applied, the H (Hue) component quantitatively represents the most dominant 'colour' based on the transformation from the captured RGB data to the target HSV colour space<sup>46</sup>, see Figure S6.

Although, individually, each approach generated good quality fits to the calibration data, it was important to establish whether a correlation existed between both detection methods. One way of achieving this was to compare the predicted pH at each unit using the derived mathematical regression models. Figure S7 presents a plot of the predicted pH using the camera model against the UV-vis model at 832 nm. Clearly, a linear correlation exists when comparing both approaches with a good fit resulting ( $R^2 = 0.98$ ,  $n = 18$ ). Moreover, the difference in slope between this linear fit and the ideal slope (slope = 1) is relatively small at 0.021, suggesting there is little bias or skewness between the two data sets. The correlation between the camera and the UV-Vis model at 605 nm was also investigated. Similar accuracies were achieved with  $R^2 = 0.98$  and a difference to the ideal slope of 0.025. From Figure S7 it can be seen that the goodness of fit of the correlation decreases above c.a. pH 7. This arises from the increasingly small absorbance (colour changes) occurring above this value, see Figure 4 (inset). Despite this, it is interesting to note that the camera and the spectrometer data remain reasonably well correlated above pH 7, although the scatter is understandably greater, see ESI† - Figure S7.

### Gradient pH measurements

The main advantage of the digital camera over the spectrometer lies in its ability to rapidly generate spatially distributed information. This should enable the camera to dynamically track changes in pH along the entire length of the fluidic channel. To test this thesis, the microchannel was filled with a pH 3 solution and a second solution of pH 6.5 was introduced at one end, as described in the experimental section and ESI†. The solutions were allowed to diffuse until a pH gradient visually appeared whereupon an image was captured (Figure 5).

Following the image processing and data extraction as described above, the images were white balanced and the Hue values at each localised point normalised with respect to the colour reference patches, as described previously for the calibration process. Using the calibration model derived from the sigmoidal regression analysis, the localised Hue values were mapped to their corresponding pH concentrations and a plot of pH concentration over the length of the channel was derived. To reduce noise, a smoothing algorithm based on the Savitzky-Golay filter<sup>62</sup> was applied to the data set. For both Figure 5b and Figure 5c, labels are present to denote discrete points along the flow path *i.e.* points of maximum curvature along the four considered flow bends.

It can be seen visually from Figure 5b that the pH varies

significantly between points '2' and '3' as reflected in the colour gradient. Correspondingly, the analysis presented (Figure 5c) shows a dramatic change in pH from *ca.* pH 3 at '2' to *ca.* pH 6.5 at, and beyond, point '3'. Figure 5c shows the resulting pH gradient as estimated by processing the colour image with the digital camera algorithm. Close examination of the image reveals the presence of small bubbles, which manifest as slight inconsistencies in the unsmoothed pH data in Figure 5c.

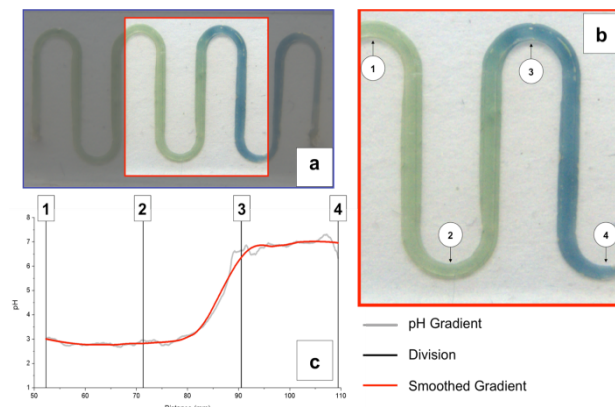


**Figure 5.** (a) Images showing a pH gradient along the microfluidic channel reflected in the changing colour of the PANi coating, red box shows a magnified section in (b), which also identifies specific locations (1-4) highlighted in (c), Plot of the pH gradient along the flow channel generated from the image. The grey line is the raw data from the analysis; the red line has been smoothed using the Savitsky-Golay algorithm.

To demonstrate the capabilities of the digital imaging approach, changes in the pH along the entire channel were tracked using low-cost digital video imaging, see supplementary information (ESI† - Video 3). In this example, the image section under analysis is bounded by a red square and also enlarged (shown in the top left corner). In addition, a dynamic plot is presented on the right hand side of the video showing the change in pH along the channel. Although the data in Figure 5a and ESI† - Video 3 represents the pH dynamics of the channel at a single point in time, this process can be easily expanded to enable pH variations to be tracked dynamically along the entire microfluidic system as a function of time.

This capability could have a substantial impact in many areas. For instance, a number of chemical reactions are time critical and require precision when introducing a reagent. By coupling a microfluidic system, PANi and a low cost colour camera, a miniaturised and cost effective solution can be achieved for many chemical and biochemical sensing scenarios that rely on a localised pH to drive the reaction. The speciation state of multi-basic acids, or of amino acids could be inferred from a knowledge of pH gradients. Mixing processes involving buffers could be tracked to identify locations of optimum pH for particular processes, and to explore how these locations can be moved, expanded or contracted prior to addition of active reagents. Furthermore, the rapid improvement in price-performance in digital photography through the development of sophisticated, miniaturised and low cost CCD sensors<sup>63-65</sup> and its increasing integration with mobile phones, provides a powerful technology platform for many new applications. However, while tremendous potential impact of integration of chemical/biological measurements with digital imaging and communications is

compelling, for example, in tele-health and personal (point-of-need) diagnostics, the route to winning applications is not clear. Hence, companies like Nokia are sponsoring global competitions with very significant prizes to generate ideas from which they will select the best possible candidate applications<sup>66</sup>. This activity emphasises the rising importance of applying digital imaging to analytical measurements.

## Conclusions

A new, simple, and fast photometric method to measure pH using PANi based coatings in microfluidic devices is presented. pH measurements were performed in continuous flow mode using fiber-optic light guides aligned to the device using an in-house made cell. The main advantage of these sensors is that no reagent indicator is needed to measure the pH, because the PANi acts as the indicator itself, reducing the complexity of pH detection inside microchannels. The functionalisation process is easy and highly reproducible from microdevice to microdevice and over the whole microchannel length. Moreover, it can be easily achieved using different materials as such glass, PDMS or any other material that allows the introduction of hydroxyl groups on the surface, necessary for the present silanisation procedure. Although the time for functionalisation is rather long (~22 h), the polyaniline functionalised micro-channels are suitable for multiple uses since the coating can be easily regenerated by passing an acidic solution (HCl solution, pH 2) inside the channel. PANi coated microchannels present long-term stability and reproducibility, can be stored at room temperature, exposed to air, empty or filled with a pH 2 solution for over two months without any deterioration in sensor performance.

Since this technique is based on pH responsive coatings, at present, it is not suitable for 3D pH sensing in microchannels but rather 2D (along the length and width of the channel) pH sensing. However, when coupled with imaging techniques, this approach offers a low cost, accurate approach for the tracking of the 2D temporal and spatial dynamics of pH changes along an entire microfluidic channel in real-time, without the need to add a pH sensitive dye to the liquid phase in the channel. The approach of using the colour camera for pH mapping is generic and could be applied for a wide variety of pH responsive systems.

## Acknowledgements

The project has been carried out with the support of the Irish Research Council (IRC) - Embark Initiative and Science Foundation Ireland under the CLARITY initiative, grant 07/CE/I1147.

## Notes and references

CLARITY: Centre for Sensor Web Technologies, National Centre for Sensor Research, Dublin City University, Dublin, Ireland, Fax: +353 1 700 7995, Tel: +353 1 700 7699; \*E-mail: fernando.lopez@dcu.ie ;

† Electronic Supplementary Information (ESI) available: Video 1 and Video 2 are showing the rapid colour change of the polyaniline coating when solutions of different pHs are passed through the microchannel. In Video 3, using image processing techniques, pH is successfully mapped when a pH gradient is induced inside the polyaniline modified microchannel. See DOI: 10.1039/b000000x/

1. K. Pasztor, A. Sekiguchi, N. Shimo, N. Kitamura and H. Masuhara, *Sens. Actuators, B*, 1993, **12**, 225-230.
2. V. K. Khanna, *Indian Journal of Pure & Applied Physics*, 2012, **50**, 199-207.
3. B. Nemeth, S. Tsuda, C. Busche, L. Cronin and D. R. S. Cumming, *Electron. Lett*, 2012, **48**, 143-U120.
4. Y. L. Chin, J. C. Chou, T. P. Sun, W. Y. Chung and S. K. Hsiung, *Sens. Actuators, B*, 2001, **76**, 582-593.
5. Y. Cheng, X. Luo, J. Betz, S. Buckhout-White, O. Bekdash, G. F. Payne, W. E. Bentley and G. W. Rubloff, *Soft Matter*, 2010, **6**, 3177-3183.
6. T. Gunnlaugsson, P. E. Kruger, P. Jensen, J. Tierney, H. D. P. Ali and G. M. Hussey, *J. Org. Chem.*, 2005, **70**, 10875-10878.
7. N. Klauke, P. Monaghan, G. Sinclair, M. Padgett and J. Cooper, *Lab Chip*, 2006, **6**, 788-793.
8. X. Ge, Y. Kostov, L. Tolosa and G. Rao, *Anal. Chim. Acta*, 2012, **734**, 79-87.
9. A. Richter, G. Paschew, S. Klatt, J. Lienig, K.-F. Arndt and H.-J. P. Adler, *Sensors*, 2008, **8**, 561-581.
10. Q. T. Trinh, G. Gerlach, J. Sorber and K.-F. Arndt, *Sens. Actuators, B*, 2006, **117**, 17-26.
11. Y. Cheng, P. Xiong, C. S. Yun, G. F. Strouse, J. P. Zheng, R. S. Yang and Z. L. Wang, *Nano Lett.*, 2008, **8**, 4179-4184.
12. C. N. Tsai, J. C. Chou, T. P. Sun and S. K. Hsiung, *Sens. Actuators, B*, 2005, **108**, 877-882.
13. W.-D. Huang, H. Cao, S. Deb, M. Chiao and J. C. Chiao, *Sensors and Actuators a-Physical*, 2011, **169**, 1-11.
14. S. Martellucci, A.N. Chester and A. G. Mignani, *Springer, New York, USA*, 2000.
15. R. M. Wolthuis, D. Saaski, E. Hartl, J. Mitchell, G., *IEEE Trans. Biomed. Eng.*, 1992, **39**, 531 - 537.
16. F. Buchholz, N. Buschmann and K. Cammann, *Sens. Actuators, B*, 1992, **9**, 41-47.
17. B. Kuswandi and R. Narayanaswamy, *Fresenius J. Anal. Chem.*, 1999, **364**, 605-607.
18. R. W. Sabnis, S. Sanders; and L. Dempsey, *Handbook of Acid-Base Indicators*, CRC Press, 2007.
19. Z. F. Ge, C. W. Brown, L. F. Sun and S. C. Yang, *Anal. Chem.*, 1993, **65**, 2335-2338.
20. E. K. Asijati, B.; Arifah, N.F.; Kurniawati, Y.I.; Gani, A.A., *Sensors and the International Conference on new Techniques in Pharmaceutical and Biomedical Research, 2005 Asian Conference on 2005*, 111 - 114
21. J. X. Huang, S. Virji, B. H. Weiller and R. B. Kaner, *J. Am. Chem. Soc.*, 2003, **125**, 314-315.
22. L. Florea, A. Hennart, D. Diamond and F. Benito-Lopez, *Sens. Actuators B: Chem.*, 2012, **175**, 92-99.
23. L. Florea, F. Benito-Lopez, A. Hennart and D. Diamond, *Procedia Engineering*, 2011, **25**, 1545 - 1548.
24. J. Miwa, Suzuki, Y., Kasagi, N., *J. Microelectromech. Syst.*, 2008, **17**, 611-622.
25. P. Mela, S. Onclin, M. H. Goedbloed, S. Levi, M. F. Garcia-Parajo, N. F. van Hulst, B. J. Ravoo, D. N. Reinhoudt and A. van den Berg, *Lab Chip*, 2005, **5**, 163-170.

26. L. Basabe-Desmonts, F. Benito-Lopez, H. J. G. E. Gardeniers, R. Duwel, A. van den Berg, D. N. Reinhoudt and M. Crego-Calama, *Anal. Bioanal. Chem.*, 2008, **390**, 307-315.
27. F. Benito-Lopez, S. Scarmagnani, Z. Walsh, B. Paull, M. Macka and D. Diamond, *Sens. Actuators, B*, 2009, **140**, 295-303.
28. K. T. Lau, R. Shepherd, D. Diamond and D. Diamond, *Sensors*, 2006, **6**, 848-859.
29. F. A. A. Matias, M. Vila and M. Tubino, *Sens. Actuators, B*, 2003, **88**, 60-66.
30. G. J. Schmidt and R. P. W. Scott, *Analyst*, 1984, **109**, 997-1002.
31. J. R. Clinch, P. J. Worsfold and H. Casey, *Anal. Chim. Acta*, 1987, **200**, 523-531.
32. P. C. Hauser, S. S. Tan, T. J. Cardwell, R. W. Cattrall and I. C. Hamilton, *Analyst*, 1988, **113**, 1551-1555.
33. K. S. Johnson, C. L. Beehler and C. M. Sakamotoarnold, *Anal. Chim. Acta*, 1986, **179**, 245-257.
34. D. Betteridge, W. C. Cheng, E. L. Dagless, P. David, T. B. Goad, D. R. Deans, D. A. Newton and T. B. Pierce, *Analyst*, 1983, **108**, 1-16.
35. M. A. Feres and B. F. Reis, *Talanta*, 2005, **68**, 422-428.
36. K. T. Lau, S. Baldwin, R. L. Shepherd, P. H. Dietz, W. S. Yezunis and D. Diamond, *Talanta*, 2004, **63**, 167-173.
37. K. T. Lau, S. Baldwin, M. O'Toole, R. Shepherd, W. J. Yezunis, S. Izuo, S. Ueyama and D. Diamond, *Anal. Chim. Acta*, 2006, **557**, 111-116.
38. M. O'Toole, K.-T. Lau, B. Shazmann, R. Shepherd, P. N. Nesterenko, B. Paull and D. Diamond, *Analyst*, 2006, **131**, 938-943.
39. S. M. Barnard and D. R. Walt, *Nature*, 1991, **353**, 338-340.
40. I. Alexandre, S. Hamels, S. Dufour, J. Collet, N. Zammateo, F. De Longueville, J. L. Gala and J. Remacle, *Anal. Biochem.*, 2001, **295**, 1-8.
41. L. Byrne, J. Barker, G. Pennarun-Thomas, D. Diamond and S. Edwards, *TrAC, Trends Anal. Chem.*, 2000, **19**, 517-522.
42. L. Byrne, K. T. Lau and D. Diamond, *Irish Journal of Agricultural and Food Research*, 2003, **42**, 119-129.
43. A. Lapresta-Fernandez and L. F. Capitan-Vallvey, *Anal. Chim. Acta*, 2011, **706**, 328-337.
44. C. Fay, K.-T. Lau, S. Beirne, C. O. Conaire, K. McGuinness, B. Corcoran, N. E. O'Connor, D. Diamond, S. McGovern, G. Coleman, R. Shepherd, G. Alici, G. Spinks and G. Wallace, *Sens. Actuators, B*, 2010, **150**, 425-435.
45. K. Cantrell, M. M. Erenas, I. de Orbe-Paya and L. F. Capitan-Vallvey, *Anal. Chem.*, 2010, **82**, 531-542.
46. A. R. Smith, *SIGGRAPH Comput. Graph.*, 1978, **12**, 12-19.
47. A. B. Shirrao and R. Perez-Castillejos, *Chips & Tips*, 17 May 2010.
48. J. F. Qiang, Z. H. Yu, H. C. Wu and D. Q. Yun, *Synth. Met.*, 2008, **158**, 544-547.
49. C. G. Wu and J. Y. Chen, *Chem. Mater.*, 1997, **9**, 399-&.
50. J. Dambrine, B. Geraud and J. B. Salmon, *New J. Phys.*, 2009, **11**.
51. K. Berrada, S. Quillard, G. Louarn and S. Lefrant, *Synth. Met.*, 1995, **69**, 201-204.
52. M. Bartonek, N. S. Sariciftci and H. Kuzmany, *Synth. Met.*, 1990, **36**, 83-93.
53. A. Hugotlegoff and M. C. Bernard, *Synth. Met.*, 1993, **60**, 115-131.
54. J. X. Huang, *Pure and Applied Chemistry*, 2006, **78**, 15-27.
55. J. Huang, S. Virji, B. H. Weiller and R. B. Kaner, *Chemistry-a European Journal*, 2004, **10**, 1315-1319.
56. S. Virji, J. D. Fowler, C. O. Baker, J. X. Huang, R. B. Kaner and B. H. Weiller, *Small*, 2005, **1**, 624-627.
57. E. Pringsheim, E. Terpetschnig and O. S. Wolfbeis, *Anal. Chim. Acta*, 1997, **357**, 247-252.
58. U. W. Grummt, A. Pron, M. Zagorska and S. Lefrant, *Anal. Chim. Acta*, 1997, **357**, 253-259.
59. J. C. Chiang and A. G. Macdiarmid, *Synth. Met.*, 1986, **13**, 193-205.
60. A. J. Epstein, J. M. Ginder, F. Zuo, R. W. Bigelow, H. S. Woo, D. B. Tanner, A. F. Richter, W. S. Huang and A. G. Macdiarmid, *Synth. Met.*, 1987, **18**, 303-309.
61. A. W. Martinez, S. T. Phillips, G. M. Whitesides and E. Carrilho, *Anal. Chem.*, 2010, **82**, 3-10.
62. A. Savitzky and M. J. E. Golay, *Anal. Chem.*, 1964, **36**, 1627-&.
63. H. Tamayama, K. Ito and T. Nishimura, Technology trends of high-definition digital still camera systems, 2002.
64. P. Maxwell, Test for low cost CMOS image sensors, 2005.
65. F. Xiao, X. Zhang and B. Fowler, Color processing in camera phones: How good does it need to be?, 2005.
66. <http://www.nokiasensingxchallenge.org/>.